Hindawi
Geofluids
Volume 2021, Article ID 9945494, 19 pages
https://doi.org/10.1155/2021/9945494

Research Article

Pore Structure and Fractal Character of Lacustrine Oil-Bearing Shale from the Dongying Sag, Bohai Bay Basin, China

Pengfei Zhang,[1,2] **Shuangfang Lu**,[2] **Zhiping Zeng**,[3] **Xiangchun Chang**,[1] **Junqian Li**,[2] **Guo Chen**,[1] **Junjian Zhang**,[1] **Zizhi Lin**,[2] **and Jijun Li**[2]

[1]*College of Earth Science and Engineering, Shandong University of Science and Technology, Qingdao, 266590 Shandong, China*
[2]*Key Laboratory of Deep Oil and Gas, China University of Petroleum (East China), Qingdao, 266580 Shandong, China*
[3]*Research Institute of Exploration and Development, Shengli Oilfield Company, Sinopec, Dongying, 257000 Shandong, China*

Correspondence should be addressed to Shuangfang Lu; lushuangfang@upc.edu.cn

Received 25 March 2021; Accepted 17 May 2021; Published 5 July 2021

Academic Editor: Shansi Tian

To better understand the pore structure and fractal character of lacustrine shales and their influence on liquid hydrocarbon occurrences, in this study, a total of 29 lacustrine oil-bearing shale samples collected from the Shahejie Formation in the Dongying Sag, Bohai Bay Basin, were investigated based on nitrogen adsorption (NGA) analysis combined with TOC, Rock-Eval pyrolysis, X-ray diffraction (XRD), and field emission-scanning electron microscopy (FE-SEM) experiments. The relationships among the compositions (TOC, minerals, and oil content), pore structures, and fractal dimensions of the lacustrine shale samples were discussed. The results showed that the adsorption and fractal characteristics of lacustrine oil-bearing shales differ at relative pressures of 0-0.1 and 0.5-1. Two corresponding fractal dimensions D_1 and D_2 were determined by the FHH model according to the nitrogen adsorption branches. Specifically, D_1 varies from 2.4292 to 2.6109 (mean 2.5245), and D_2 varies between 2.4680 and 2.8535 (mean 2.6889). The specific surface area (SSA) ranges from 1.512 m^2/g to 34.002 m^2/g, with an average of 13.656 m^2/g, the total pore volume is between 6.0×10^{-3} cm^3/g and 48.4×10^{-3} cm^3/g (mean 24.5×10^{-3} cm^3/g), and the average pore diameter is in the range of 4.22 nm to 19.57 nm (mean 9.35 nm). Both D_1 and D_2 increase with increasing SSA and increase with decreasing average pore diameters but have no correlation with pore volume. Moreover, D_1 and D_2 exhibit positive relationships with clay minerals and negative correlations with carbonate minerals (calcite and dolomite). The relationship between fractal dimensions (D_1 and D_2) and TOC contents is expressed as a U-shaped curve, characterized by the minimum D values at approximately 3% TOC. The shale oil content is controlled by the pore structures and fractal dimensions, and lacustrine shales with lower SSAs and smaller fractal dimensions would have more free oil. Therefore, lacustrine shales in the oil window with TOC contents ranging from 2% to 4% are probably the preferred shale oil exploration target in the Shahejie Formation, Dongying Sag, Bohai Bay Basin. The results indicate that fractal analysis can provide insight into the pore structure characteristics and oil storage capacity of lacustrine shales.

1. Introduction

Due to the large amount of resources, unconventional oil and gas (including tight sands, coalbed methane, shale oil, and gas) have become an increasingly important component of global energy. In particular, the remarkable achievements of shale gas exploration and exploitation (called the "shale gas revolution") in North America have encouraged the world to explore this new energy source [1]. Meanwhile, shale oil has also been proven to have considerable resources and is considered a future worldwide energy source. Shale oil is widely distributed in continental petroliferous basins in China, and more emphasis has been gradually placed on shale oil exploration and exploitation in recent years, stimulated by insufficient shale gas reserves [2–4].

Shale oil is a complex mixture consisting of hydrocarbons, nonhydrocarbons, and asphaltenes and exists mostly in adsorbed and free states in shale pore-fracture systems [5]. Pore structure determines the content and state of shale oil. Free oil mostly occurs in larger pores, while

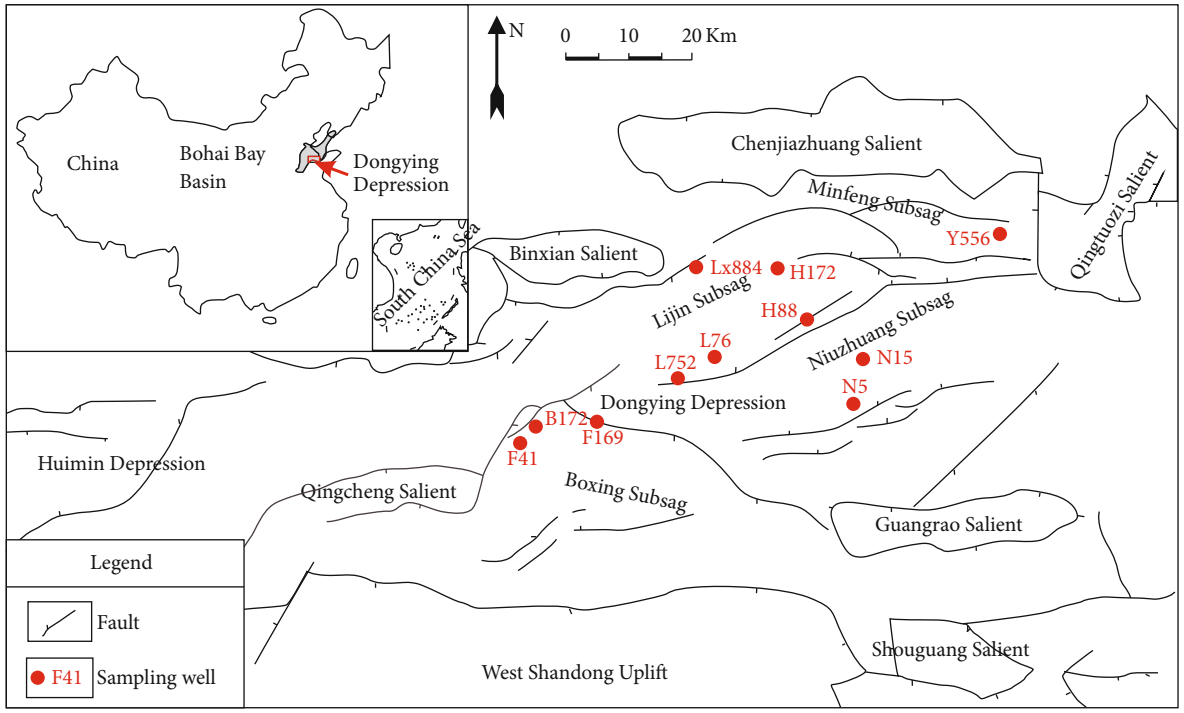

FIGURE 1: Study area geological structure and sampling locations [6, 31].

adsorbed oil primarily occurs in small pores [6, 7]. Moreover, the larger the pore volume is, the higher the content of shale oil. Previous studies have indicated that shale is a complex and heterogeneous reservoir characterized by a wide pore size distribution and large amounts of clay minerals and organic matter [8–11]. For the lacustrine shale in the oil window, clay minerals and brittle minerals (such as quartz, calcite, and dolomite) provide a main pore space rather than organic matter, which is different from marine gas shale [12]. Recently, many studies have been conducted on marine gas shale to reveal its pore structure and influence on shale gas content [13–19]. However, although previous studies have been performed to analyse the pore structure of lacustrine oil-bearing shale, it is rarely associated with shale oil content [12]. Moreover, shale oil content is also controlled by the complexity and heterogeneity of the pore structure.

At present, many specialized techniques have been developed to investigate the pore structure of shale and can usually be divided into two categories: direct imaging and indirect methods. Direct imaging methods, such as field emission-scanning electron microscopy and X-ray CT, have proven to be effective techniques to provide direct information (such as pore types and morphology) about real pore networks [11, 20, 21]. However, the pore structure of shale can be qualitatively characterized by indirect methods, such as nitrogen adsorption (NGA), mercury intrusion capillary pressure (MICP), and nuclear magnetic resonance (NMR), to obtain the pore volume, pore size distribution, specific surface area, etc. [18, 22–25]. Among these methods, NGA is considered an effective technique to characterize the micropore structure of shale [15, 16, 26–28]. The nitrogen adsorption datum suggests that shale has fractal geometries, and the fractal dimensions can be used to characterize the shale oil or gas contents [12, 13].

The main purpose of this paper is to investigate the pore structure and fractal character of lacustrine oil-bearing shales from the Shahejie Formation in the Dongying Sag, Bohai Bay Basin, based on nitrogen adsorption measurements. TOC content, Rock-Eval pyrolysis, XRD, and FE-SEM tests were also performed to discuss the relationships between the composition and pore structure and fractal dimensions of shales. Moreover, the effect of pore structure parameters and fractal dimensions on shale oil content is analysed. The results are relevant for providing insight into the pore structures and shale oil storage in lacustrine oil-bearing shale in the Dongying Sag, Bohai Bay Basin.

2. Samples and Methodology

2.1. Samples. In this study, twenty-nine lacustrine shale core samples were collected from the Paleogene Shahejie Formation of 11 shale oil boreholes in the Dongying Sag, Bohai Bay Basin (Figure 1). This sag is located in the SE of the basin with an area of approximately 5800 km^2. The upper part of the Paleogene Shahejie Formation fourth member (Es_4^U) and the lower part of its third member (Es_3^L) contain thick, organic-rich shales and are regarded as the main source rocks with excellent potential for shale oil development [29, 30]. The basic geological background of this sag has been published previously [6, 31].

2.2. Methodology

2.2.1. Experiments. A relatively complete experimental project was performed, including TOC contents, rock pyrolysis,

Table 1: Geochemical characteristics and mineral compositions of shale samples.

Sample	Depth/m	Organic matter			Mineral composition/%					
		TOC/%	S_1/mg/g	T_{max}/°C	CL	Q	O	P	C	D
B172-1	3407.4	2.06	1.5014	443	30.3	12.2	0.0	1.9	42.6	7.5
B172-2	3407.6	0.53	0.1072	450	54.8	22.9	1.0	5.8	11.0	4.5
F169-5	3761.1	0.55	0.1065	428	58.2	16.9	0.8	4.7	10.6	8.8
F169-1	3697.0	0.67	0.167	440	39.8	30.8	1.8	11.1	6.1	10.3
F169-2	3760.8	0.51	0.1008	417	36.7	24.1	1.5	10.1	16.7	5.9
H172-1	3336.8	3.15	2.0967	441	43.9	19.6	0.5	1.1	26.9	1.0
Y556-3	2970.0	2.36	1.0230	438	27.6	22.3	1.7	5.7	19.9	15.7
N15-1	3276.4	2.25	1.2164	441	25.5	13.1	1.3	6.8	41.3	8.9
H172-3S	3426.9	3.37	4.1145	441	52.6	20.9	0.5	2.0	15.2	1.9
H172-4S	3428.6	2.83	2.7574	440	50.8	27.8	0.5	2.1	9.9	5.2
LX884-1	3506.2	2.52	2.9565	443	30.0	26.0	0.2	2.7	18.7	17.5
Y556-1	2448.3	2.68	0.4580	435	37.0	20.0	1.7	2.5	31.6	0.0
Y556-2	2516.2	2.62	0.4749	437	32.8	19.8	1.8	3.0	25.6	6.9
LX884-2S	3502.4	3.73	4.6931	446	43.7	21.7	0.5	3.6	3.2	22.5
N5-4S	2605.5	1.99	0.7651	440	20.4	7.7	1.3	3.2	60.3	5.2
Y556-5S	2448.2	3.17	0.6281	433	33.4	13.8	1.6	2.1	40.2	3.6
F169-4	3757.4	1.28	4.0867	428	7.8	46.8	2.9	31.5	8.3	2.7
F41-3	2693.9	1.19	1.4087	434	13.2	33.3	8.5	32.2	8.3	4.5
F41-2	2679.3	1.66	0.2880	439	14.0	38.7	5.8	18.5	11.2	6.6
L752-3	3550.1	1.33	0.8941	445	7.7	5.8	0.1	2.2	22.0	55.8
L76-2	3780.4	0.36	0.0942	452	28.9	40.0	2.8	14.2	1.8	8.9
N5-3	2740.8	0.16	0.1232	443	2.6	43.0	5.1	16.8	14.7	14.0
N5-5S	2642.1	4.55	1.6116	423	36.8	25.8	1.0	7.1	14.6	5.0
B172-3	3405.6	0.87	0.1776	440	14.8	35.5	2.5	10.3	6.1	30.8
F169-3	3697.8	0.59	0.1163	444	58.2	16.9	0.8	4.7	10.6	8.8
H88-1	3042.6	1.44	0.2163	442	55.5	30.8	2.1	7.9	3.6	0.0
H88-2	3044.6	1.70	0.2335	443	46.2	21.3	4.7	5.5	12	5.9
L752-2	3560.1	0.60	0.1161	449	46.1	26.3	4.3	11.1	3.5	4.8
L76-1	3783.6	0.32	0.0941	463	32.1	37.7	4.8	10.5	2.3	8.3

TOC stands for total organic carbon; S_1 denotes Rock-Eval measured oil content at 573.15 K; T_{max} indicates pyrolysis hydrocarbon peak temperature; Cl, Q, O, F, C, and D represent clay minerals, quartz, orthoclase, plagioclase, carbonate, and dolomite, respectively.

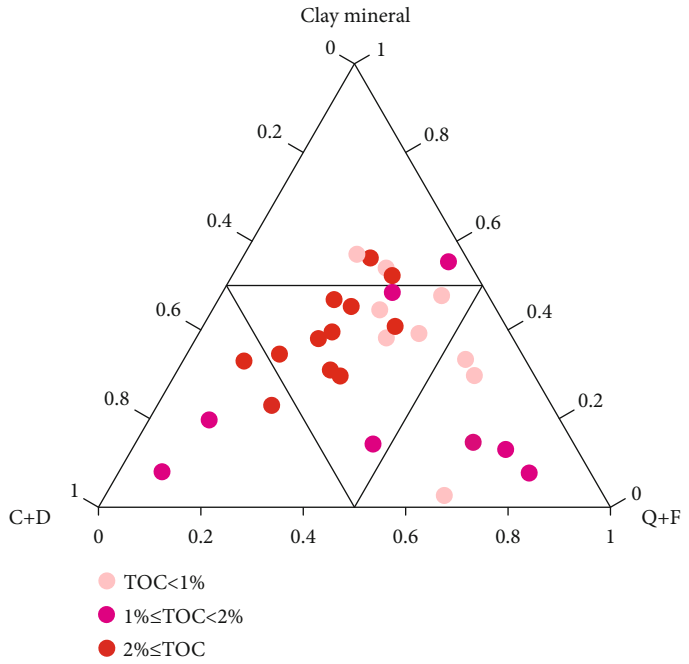

Figure 2: Shale sample mineralogical composition ternary diagram.

X-ray diffraction (XRD) analysis, field emission-scanning electron microscopy (FE-SEM), and nitrogen adsorption (NGA).

Shale core samples were crushed to 100 mesh to conduct the TOC content, rock pyrolysis, and XRD analyses. An Elab-TOC analytical instrument (Elam Analytical Instrument Co., Ltd, Suzhou, China) was used to measure the total organic carbon (TOC) of shale samples. The rock pyrolysis tests were carried out on a Rock-Eval VI instrument. The organic geochemistry parameters, including TOC, S_1 (volatile hydrocarbon content), and T_{max} (temperature of maximum pyrolysis yield), were obtained. XRD data were collected using a Bruker diffractometer to determine the mineral composition of shale samples.

An FFI Quanta 200F field emission-scanning electron microscope was employed to carry out the FE-SEM tests. The samples were cut parallel to the bedding surface and then mounted on stubs and hand-polished. Subsequently, a flat surface was obtained by argon-ion milling. In addition, prior to this processing, residual oil in shale pores was first removed using dichloromethane and acetone (3 : 1 in volume) at 0.3 MPa and 90°C for 72 h and dried at 110°C in a vacuum oven (at -0.1 MPa) for 24 h. A series of back-scattered electron (BSE) and secondary electron (SE) images of the flat surface were collected at resolutions ranging from 1.04 nm to 558 nm.

Nitrogen adsorption (NGA) experiments were conducted on a Micromeritics ASAP 2460 specific surface area and porosity analyser. Shale samples were sieved to obtain grain sizes of 40-60 mesh (0.25-0.42 mm) and then put into an oil-cleaned instrument for 72 h to remove any residual oil using the same method. Subsequently, the particle samples were dried at 383 K for 12 in a vacuum oven prior to NGA testing. Nitrogen adsorption-desorption isotherms at 77 K were collected for relative pressures (P/P_0) ranging from 0.01 to 0.993. In this paper, the total pore volume (PV), specific surface area (SSA), and average pore diameter were all obtained from the adsorption branch. PV is the single pore volume determined at a relative pressure of 0.99. SSA was calculated based on the adsorption data with relative pressures between 0.05 and 0.35 using multilayer adsorption theory (Brunauer-Emmett-Teller, BET method). The average pore diameter (d_a) was determined by PV and SSA based on the columnar model.

2.2.2. Fractal Model. The fractal model was introduced by Mandelbort [32] and is regarded as an effective method for characterizing the geometry of complex non-Euclidean shapes. The fractal dimension (D) is a quantitative parameter to indicate the roughness or complexity of the solid surface. In three dimensions, the fractal dimension values regularly vary from 2 to 3, and values closer to 3 mean increasing roughness or complexity. Several methods have been proposed to calculate the fractal dimension based on gas adsorption isotherms, while the FHH (Frenkel-Halsey-Hill) model has been proven to be the most effective and is widely used for many types of porous rocks [33, 34]. The calculation of fractal dimensions by the FHH model based on nitrogen adsorption can be described as follows [33].

$$\ln\left(\frac{V}{V_0}\right) = A\left(\ln\left(\ln\left(\frac{p_0}{p}\right)\right)\right) + C, \quad (1)$$

where V represents the nitrogen adsorbed volume at the pressure of P (the equilibrium pressure); V_o is the volume

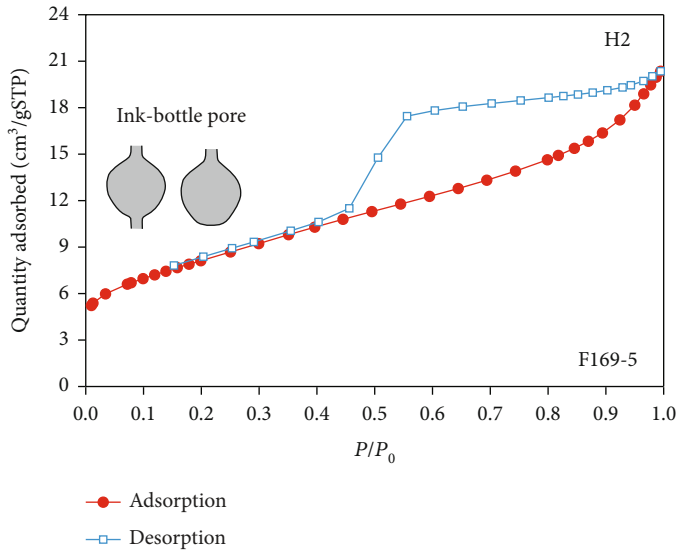

(a)

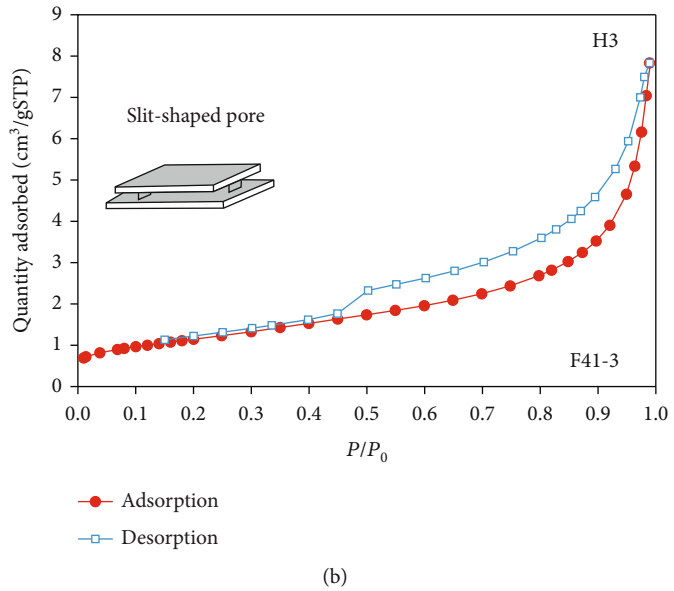

(b)

Figure 3: Continued.

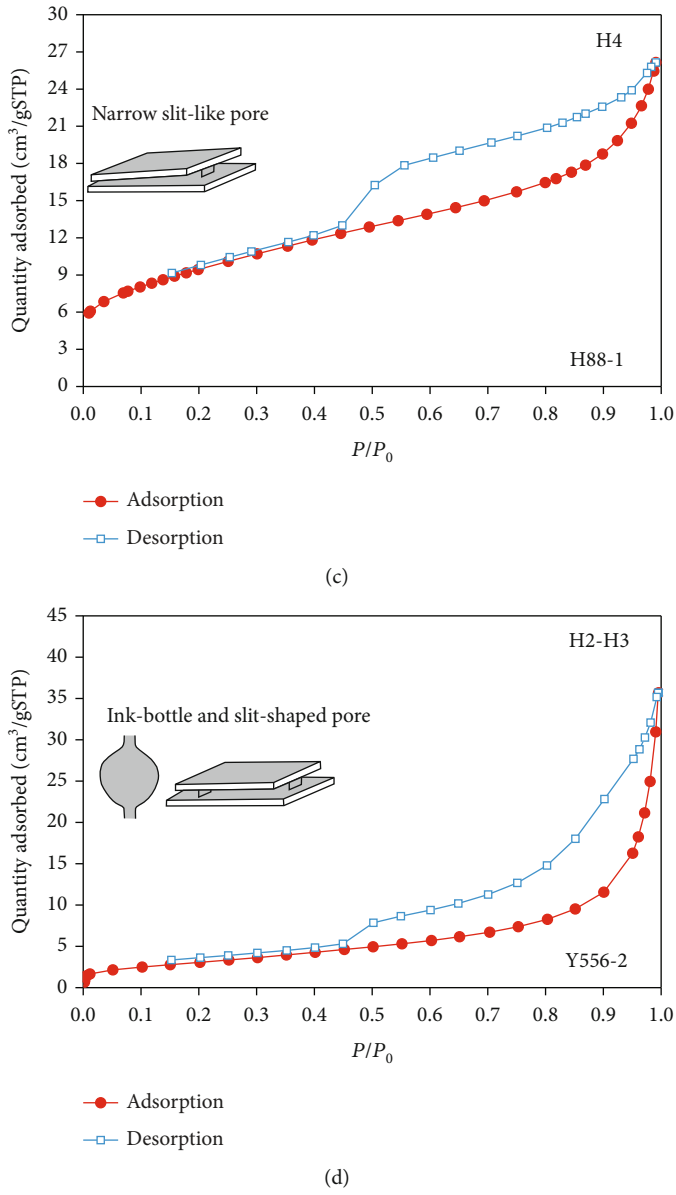

Figure 3: Nitrogen adsorption-desorption isotherms of shales.

of monolayer coverage; P_0 indicates the saturation vapor pressure of nitrogen at 77 K; and C is a constant. If the micropore structures of shales are fractal, there will be a linear relationship between $\ln(V)$ and $\ln(\ln(P_o/p))$. Fractal dimension can be derived from slope A.

$$D = A + 3. \quad (2)$$

3. Results

3.1. Organic Geochemistry and Mineralogy. The TOC contents, S_1 values, T_{max} results, and mineral percentages of the studied samples are listed in Table 1. The TOC content of shale samples varies from 0.16% to 4.55%, with an average of 1.76%. The values of S_1 were between 0.0941 mg/g and 4.6931 mg/g (mean 1.1251 mg/g). The T_{max} value ranges from 417°C to 463°C, indicating that the organic matter maturity varies from low to mature. According to Table 1, the dominant minerals in the lacustrine shales are clay minerals, quartz, and calcite. The clay mineral content ranges from 2.6% to 58.2%, with a mean of 33.84%. The average content of quartz is 24.88% (5.8%-46.8), while the calcite content is 1.8%-60.3% (mean 17.2%). Moreover, the shales contain some amounts of dolomite, plagioclase, and orthoclase, with average values of 10.43%, 8.31%, and 2.22%, respectively. According to the impact of TOC content on the hydrogen richness [35], two critical values of 1% and 2% were used as the boundary for organic-lean, organic-bearing, and organic-rich lithofacies [7] (Figure 2). With respect to these studied lacustrine shales, organic-rich shales

Table 2: Pore parameters of study samples from NGA.

Sample	Loop type	BET SSA (m^2/g)	Pore volume (10^{-3} cm^3/g)	d_a/nm	Pore percentages/%		
					<25 (nm)	25-100 (nm)	>100 (nm)
B172-1	H2	8.738	15.3	7.01	64.60	21.94	13.46
B172-2	H2	25.493	30.6	4.81	73.14	19.00	7.86
F169-5	H2	29.141	31.5	4.32	78.26	16.48	5.26
F169-1	H2	28.909	32.1	4.44	74.40	18.77	6.83
F169-2	H2	26.743	28.2	4.22	74.58	17.12	8.30
H172-1	H2	9.530	21.9	9.20	41.32	37.67	21.01
Y556-3	H2	3.347	7.2	8.61	48.78	27.97	23.25
N15-1	H2	3.9630	16.2	16.32	37.26	46.97	15.77
H172-3S	H2	4.326	12.4	11.43	40.70	36.31	22.99
H172-4S	H2	12.432	24.3	7.81	57.58	29.66	12.76
LX884-1	H2-H3	12.530	32.7	10.43	53.88	30.10	16.02
Y556-1	H2-H3	14.778	48.4	13.09	40.85	40.14	19.01
Y556-2	H2-H3	10.034	41.0	16.36	35.71	40.59	23.70
LX884-2S	H2-H3	13.198	33.5	10.17	58.99	29.02	11.99
N5-4S	H2-H3	3.065	15.0	19.57	28.92	43.78	27.30
Y556-5S	H2-H3	15.115	41.6	11.00	42.88	42.71	14.41
F169-4	H3	1.512	6.0	15.77	37.00	33.47	29.53
F41-3	H3	4.1510	12.1	11.68	40.81	38.35	20.84
F41-2	H3	10.584	22.5	8.50	48.27	34.10	17.63
L752-3	H3	2.240	6.5	11.62	41.54	31.86	26.60
L76-2	H3	12.283	27.3	8.88	61.01	26.89	12.10
N5-3	H3	5.717	12.8	8.94	47.89	28.32	23.79
N5-5S	H3	5.720	18.6	13.00	31.12	37.77	31.11
B172-3	H4	4.450	9.0	8.12	55.21	26.84	17.95
F169-3	H4	17.923	25.3	5.65	68.72	21.49	9.79
H88-1	H4	34.002	40.4	4.76	67.62	22.64	9.74
H88-2	H4	20.405	30.8	6.04	60.18	26.84	12.98
L752-2	H4	21.992	25.0	4.54	72.41	18.82	8.77
L76-1	H4	33.695	41.6	4.94	79.06	13.84	7.10

SSA is the special surface area; d_a is the average pore diameter.

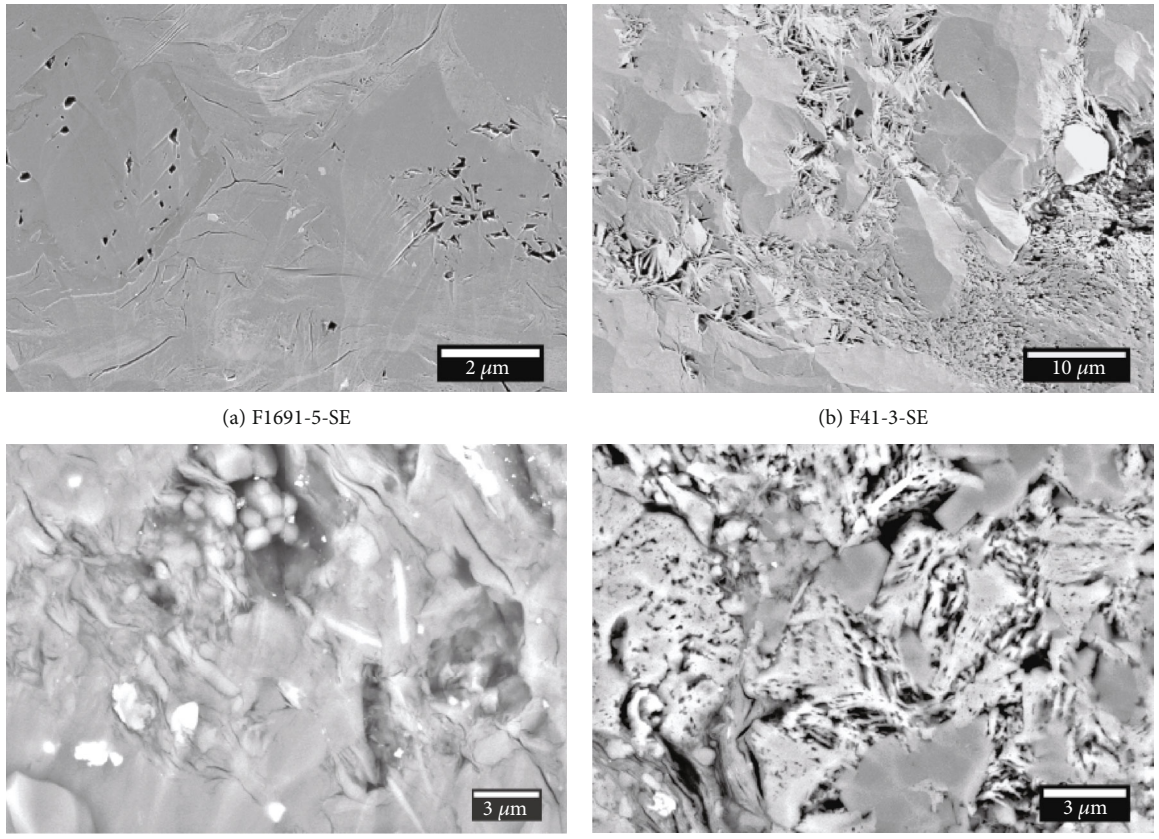

(a) F1691-5-SE (b) F41-3-SE

(c) H88-1-BSE (d) Y556-2-BSE

Figure 4: SEM images of the studied shales.

are mainly dominated by mixed minerals but are highly calcareous (calcite and dolomite), while organic-bearing shales are commonly highly calcareous or felsic (quartz and feldspar). Organic-lean shales are characterized by high felsic or clay minerals.

3.2. Nitrogen Adsorption-Desorption Isotherms. The nitrogen adsorption isotherms of some lacustrine shales are illustrated in Figure 3. The adsorption isotherms of the studied shales belong to type II on the basis of the IUPAC classification [36]. According to Figure 3, the nitrogen adsorption process can be divided into three stages. At a low relative pressure ($P/P_0 < 0.4$), the adsorption amount is low and increases slowly with increasing relative pressure, which is considered nitrogen monolayer coverage on the pore surface at this stage. Subsequently, at a medium-high relative pressure ($0.4 < P/P_0 < 0.8$), the adsorption amount approximately linearly increases as the relative pressure increases, belonging to the stage of multilayer coverage. Finally, as the relative pressure increases from 0.8 to 1.0, a significant increase in nitrogen adsorption is noted, while adsorption saturation is not achieved when the relative pressure is close to P_0 (saturation vapor pressure). Capillary condensation occurred at this stage.

In addition, at low relative pressure, the adsorption and desorption branches of the isotherms almost overlap. However, when the relative pressure is larger than 0.4, a hysteresis loop appears between the adsorption and desorption branches, which can indicate the dominant pore types in shales. According to the hysteresis loop shape of the nitrogen adsorption-desorption isotherms, the studied shales belong to three typical types and a mixed type: H2, H3, H4, and H2-H3 (Table 2). For type H2, an obvious yielding point appears in the desorption branch at a relative pressure of nearly 0.5, resulting in a hysteresis loop, which reflects the ink-bottle-shaped pores (Figure 3(a)). The corresponding SEM image shows that the pores are mainly ellipse- or polygon-shaped dissolution pores (Figure 4(a)). For type H3, the adsorption and desorption branches are nearly parallel at medium-high relative pressure and steeply increase when P approaches P_0, resulting in a narrow hysteresis loop, reflecting silt-shaped pores (Figure 3(b)). Moreover, many plate-like pores are recognized in the SEM images, which are mainly intragranular pores in clay mineral aggregates (Figure 4(b)). Type H4 can be recognized by a narrow loop and a flat adsorption-desorption isotherm, which is associated with the narrow silt-shaped pores in clay mineral aggregates (as shown in Figures 3(c) and 4(c)). For mixed types H2-H3, the desorption branch appears upper convex and forms an obvious hysteresis loop, which is the main characteristic of both types H2 and H3, indicating that both ink-bottle and silt-shaped pores exist (Figure 3(d)). Both ellipse-

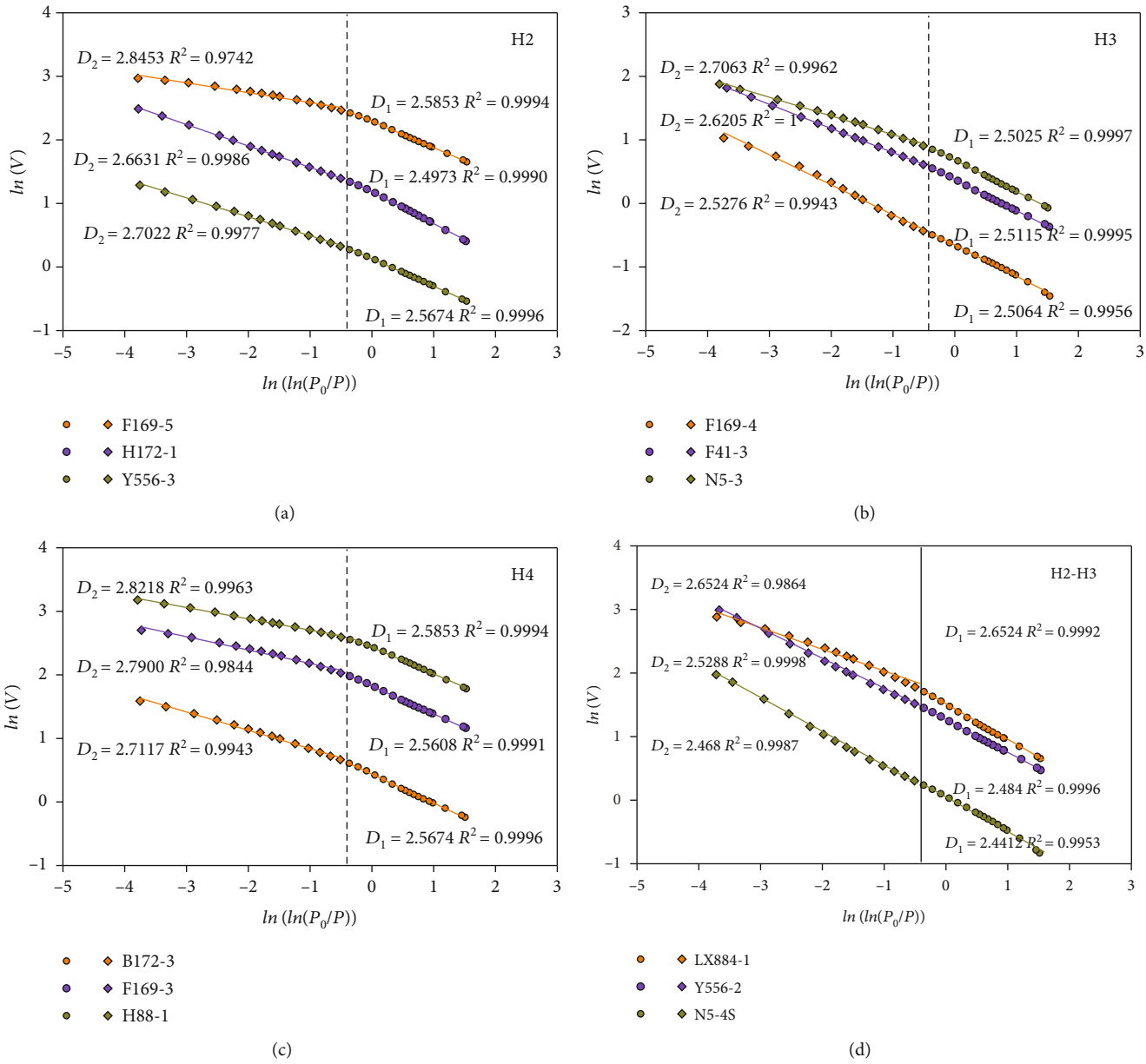

Figure 5: Fractal calculation results from ln (V) vs. ln (ln (P/P_0)) of nitrogen adsorption from shales.

or polygon-shaped dissolution pores in carbonate minerals and plate-like pores in clay mineral aggregates can be observed in large numbers (as shown in Figure 4(d)). It can be concluded that pores generated from carbonate mineral dissolution are generally ink-bottle shaped and that the intragranular pores in clay mineral aggregates are mainly slit-shaped.

3.3. Micropore Structure. The micropore structure parameters, including the SSA, pore volume, d_a, and pore percentages, are listed in Table 2. The SSA values of the studied lacustrine shales range from 1.512 m^2/g to 34.002 m^2/g with an average of 13.656 m^2/g. Type H4 shales have the largest SSA, followed by types H2, H2-H3, and H3. The pore volume is between 6.0×10^{-3} cm^3/g and 48.4×10^{-3} cm^3/g (mean 24.5×10^{-3} cm^3/g). The d_a values vary from 4.22 nm to 19.57 nm, with a mean of 9.35 nm, larger than those of marine shales from the Lower Cambrian Qiongzhusi Formation and Lower Silurian Longmaxi Formation [15, 16]. Type H3 and H2-H3 shales have larger d_a values, with mean values of 11.20 nm and 13.44 nm, respectively. In this study, pore size classification of the shale oil reservoir proposed by Zhang et al. [37] was adopted. For the studied shales, pores less than 25 nm occupy the largest proportion (mean 53.88%) of the pore volume, especially types H2 and H4. The pores between 25 nm and 100 nm make the second largest contribution, with an average content of 29.64%. The larger average pore diameter and the higher content of pores larger than 100 nm of types H3 and H2-H3 lead

Table 3: Fractal dimensions derived from the FHH model.

Sample	$P/P_0 < 0.5$			$P/P_0 > 0.5$		
	Fitting equation	R^2	D_1	Fitting equation	R^2	D_1
B172-1	$y = -0.5414x + 1.1167$	0.9996	2.4586	$y = -0.2613x + 1.2414$	0.9874	2.7387
B172-2	$y = -0.3922x + 2.197$	0.9968	2.6078	$y = -0.1598x + 2.2208$	0.9933	2.8402
F169-5	$y = -0.4147x + 2.2918$	0.9994	2.5853	$y = -0.1547x + 2.4333$	0.9742	2.8453
F169-1	$y = -0.3949x + 2.2773$	0.9994	2.6051	$y = -0.1612x + 2.3954$	0.9869	2.8388
F169-2	$y = -0.3891x + 2.1943$	0.9990	2.6109	$y = -0.1465x + 2.3097$	0.9851	2.8535
H172-1	$y = -0.5024x + 1.184$	0.9989	2.4976	$y = -0.3369x + 1.2306$	0.9997	2.6631
Y556-3	$y = -0.4326x + 0.1303$	0.9996	2.5674	$y = -0.2978x + 0.1941$	0.9977	2.7022
N15-1	$y = -0.5012x + 0.3293$	0.9998	2.4988	$y = -0.5071x + 0.3043$	0.9989	2.4929
H172-3S	$y = -0.5073x + 0.3973$	0.9978	2.4927	$y = -0.3863x + 0.4271$	0.9995	2.6137
H172-4S	$y = -0.5099x + 1.4575$	0.9994	2.4901	$y = -0.299x + 1.5664$	0.9923	2.7010
LX884-1	$y = -0.5592x + 1.5004$	0.9992	2.4408	$y = -0.3476x + 1.6701$	0.9864	2.6524
Y556-1	$y = -0.5008x + 1.6486$	0.9999	2.4992	$y = -0.4263x + 1.6514$	0.9995	2.5737
Y556-2	$y = -0.516x + 1.2642$	0.9996	2.4840	$y = -0.4712x + 1.266$	0.9998	2.5288
LX884-2S	$y = -0.5708x + 1.5555$	0.9998	2.4292	$y = -0.3498x + 1.7486$	0.9718	2.6502
N5-4S	$y = -0.5588x + 0.0648$	0.9953	2.4412	$y = -0.532x - 0.0007$	0.9987	2.468
Y556-5S	$y = -0.4772x + 1.6506$	0.9994	2.5228	$y = -0.4032x + 1.6605$	0.9999	2.5968
F169-4	$y = -0.4936x - 0.6543$	0.9956	2.5064	$y = -0.4724x - 0.692$	0.9934	2.5276
F41-3	$y = -0.4885x + 0.3735$	0.9995	2.5115	$y = -0.3795x + 0.4199$	1.0000	2.6205
F41-2	$y = -0.4651x + 1.293$	0.9997	2.5349	$y = -0.3105x + 1.3458$	0.9999	2.6895
L752-3	$y = -0.506x - 0.2505$	0.9996	2.494	$y = -0.3656x - 0.1767$	0.9980	2.6344
L76-2	$y = -0.47817x + 1.48$	0.9940	2.5213	$y = -0.3066x + 1.6616$	0.9810	2.6934
N5-3	$y = -0.4975x + 0.6844$	0.9997	2.5025	$y = -0.2937x + 0.7892$	0.9962	2.7063
N5-5S	$y = -0.4543x + 0.6536$	0.9897	2.5457	$y = -0.4135x + 0.5976$	0.9985	2.5865
B172-3	$y = -0.4577x + 0.4388$	0.9986	2.5423	$y = -0.2883x + 0.5515$	0.9943	2.7117
F169-3	$y = -0.4392x + 1.8241$	0.9991	2.5608	$y = -0.21x + 1.9709$	0.9844	2.7900
H88-1	$y = -0.4201x + 2.4361$	0.9979	2.5799	$y = -0.1782x + 2.526$	0.9963	2.8218
H88-2	$y = -0.4619x + 1.9346$	0.9986	2.5381	$y = -0.2365x + 2.0188$	0.9978	2.7635
L752-2	$y = -0.4162x + 2.0063$	0.9991	2.5838	$y = -0.1627x + 2.1242$	0.9892	2.8373
L76-1	$y = -0.4408x + 2.4653$	0.9980	2.5592	$y = -0.1647x + 2.6669$	0.9518	2.8353

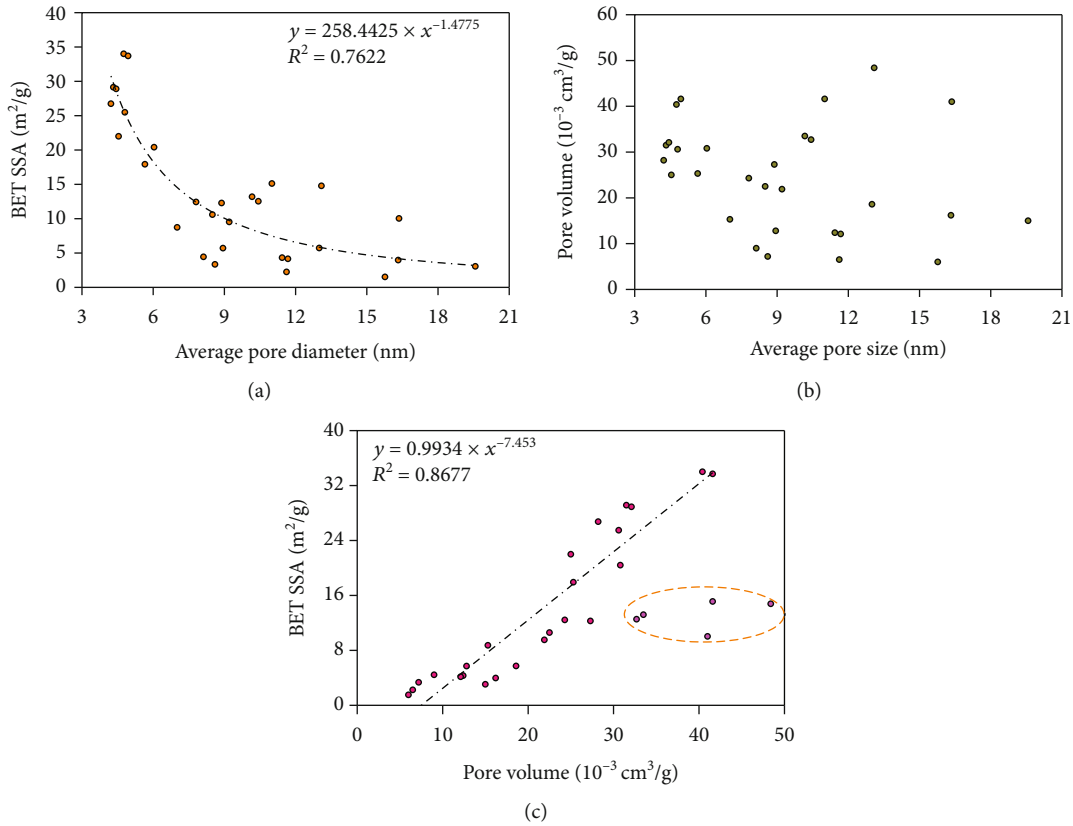

Figure 6: Relationship among various pore structure parameters.

to these two types of shale being more conducive to the storage and flow of shale oil.

3.4. Fractal Dimensions from Nitrogen Adsorption. The FHH plots of some studied shales with different types of hysteresis loops are shown in Figure 5. Two distinct linear segments at relative pressures (P/P_0) of 0-0.5 and 0.5-1 are identified, which indicate that there are two types of gas adsorption mechanisms occurring in these two regions. At a relative pressure of 0-0.5, nitrogen monolayer and multilayer coverage mainly occurred. Thus, the fractal dimension D_1 reflects the surface fractal dimension [33]. However, nitrogen capillary condensation mainly occurred at a relative pressure of 0.5-1, so the fractal dimension D_2 reflected the pore structure fractal dimension.

The equations of fitting straight lines and fractal dimensions at P/P_0 values of 0-0.5 and 0.5-1 are shown in Table 3. The fractal dimension D_1 values of the studied shale range from 2.4292 to 2.6109, with a mean value of 2.5245, which is similar to the D_1 (mean 2.5990) of marine shale from the lower Cambrian Qiongzhusi Formation [16] but larger than the D_1 (mean 2.3815) of lacustrine shale from the Qingshankou Formation of the Songliao Basin [12]. The fractal dimension D_2 values are between 2.4680 and 2.8535, with an average of 2.6889, which is similar to the D_2 (mean 2.6892) of the Qingshankou shale but less than the D_2 (mean 2.8022) of the Qiongzhusi shale (mean 2.8022). Thus, the pore surface of the studied shale is more complex and heterogeneous than that of the Qingshankou shale in the Songliao Basin.

4. Discussion

Fractal characteristics and pore structures are generally controlled by the lacustrine shale composition, including TOC content and minerals, which also affect the content and mobility of shale oil. Therefore, the factors of pore structure and fractal dimensions will be discussed. Moreover, the oil contents affected by pore structures and fractal dimensions are also revealed.

4.1. Factors Effect on Pore Structure. The relationships among the various pore structure parameters of the studied shale are shown in Figures 6 and 7. The average pore diameter shows a negative correlation with SSA but no correlation with pore volume (Figures 6(a) and 6(b)). There are positive correlations between SSA and pores less than 25 nm and pores between 25 and 100 nm but a negative correlation with pores larger than 100 nm (Figure 7(a)). Thus, shales with larger average pore diameters would also have more pores larger than 100 nm, resulting in a low SSA. Pore volumes are positively correlated with pores less than 25 nm but negatively correlated with pores larger than 100 nm. Meanwhile, pore volume

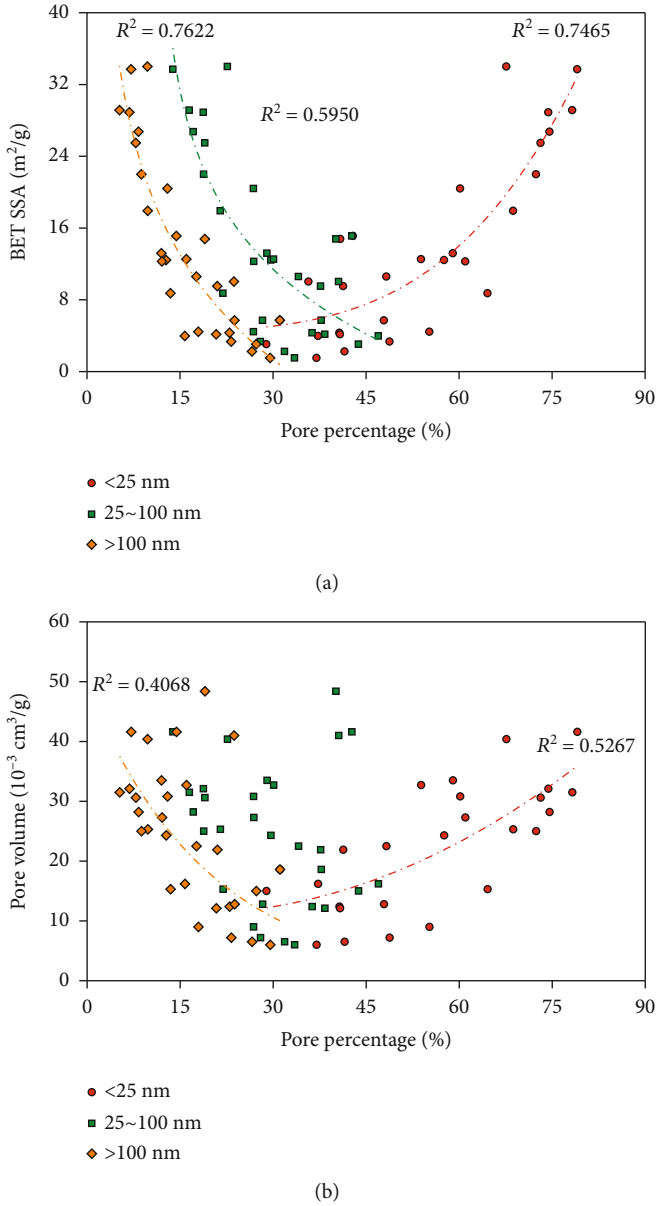

Figure 7: Relationships between specific surface area (a) and pore percentages and the relationships between pore volume (b) and pore percentages.

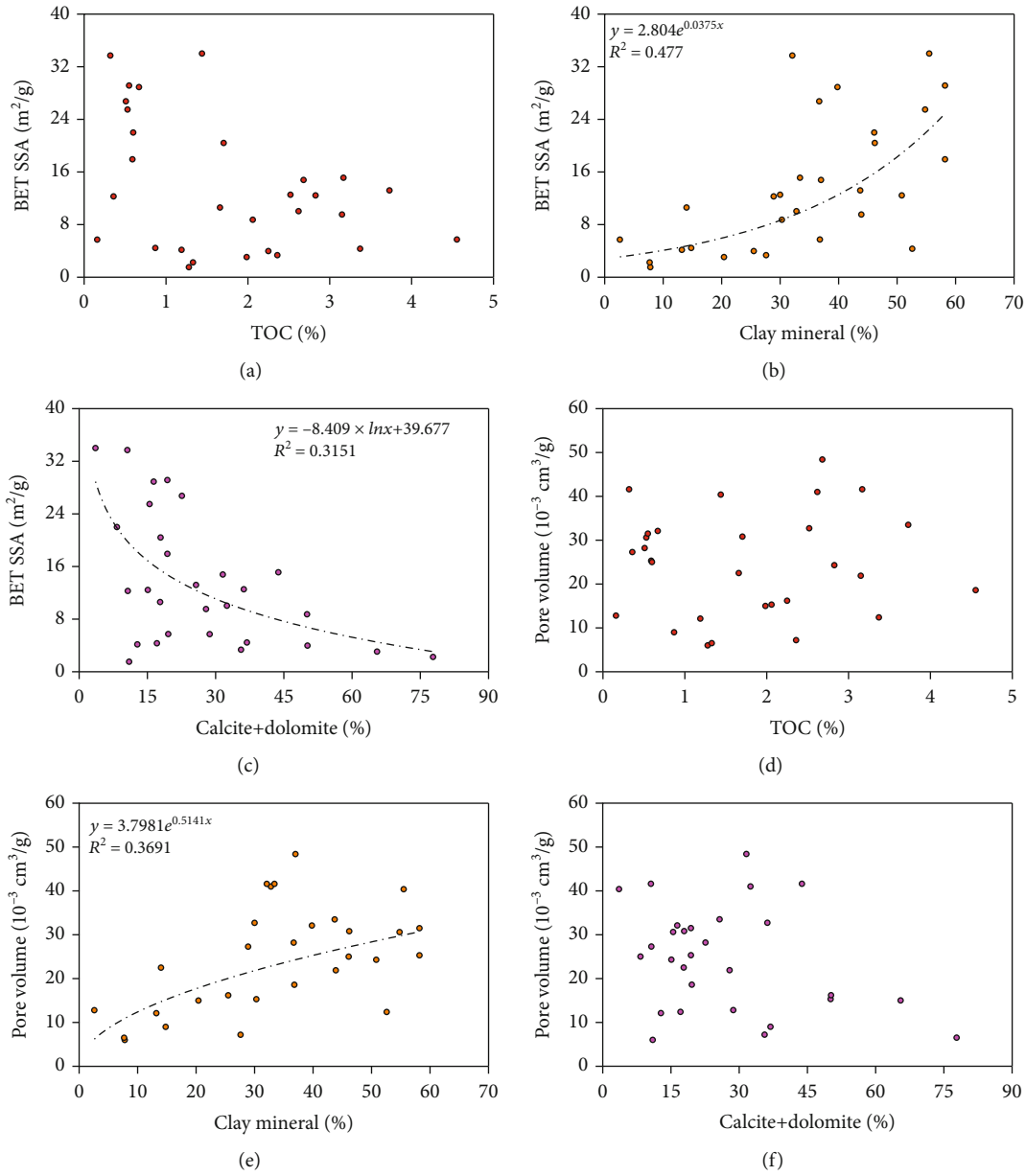

Figure 8: Relationships between the specific surface area and the TOC (a), clay minerals (b), and calcite +dolomite (c) and relationships between the pore volume and the TOC (d), clay minerals (e), and calcite +dolomite (f).

has no apparent relationship with pores between 25 and 100 nm, which means that there is no apparent correlation between pore volume and average pore diameter. The SSA is positively correlated with pore volume except for some samples with many dissolution pores. The secondary dissolution pores in the carbonate minerals generally have larger pore sizes (as shown in Figure 4(d)). The dissolution pores make a significant contribution to the pore volume rather than the SSA. Thus, shales with many dissolution pores are characterized by a high pore volume but a low SSA.

The influences of TOC and clay and carbonate minerals (calcite and dolomite) on the structural parameters are illustrated in Figure 8. The SSA and pore volume have no apparent relationship with the TOC content (Figures 8(a) and 8(d)), which is different from the overmature marine shale in South China. The reason is that there are few organic pores in the shale within the oil window, which makes organic matter have no apparent contribution to the SSA and pore volume of the studied lacustrine shale. The slightly positive correlations between the clay mineral component, SSA, and pore volume suggested that clay minerals are the contributor to the SSA and pore volume (as shown in Figures 8(b) and 8(e)). The SEM images also illustrate that there are many plate-like intragranular pores in clay minerals (Figures 4(b) and 4(c)).

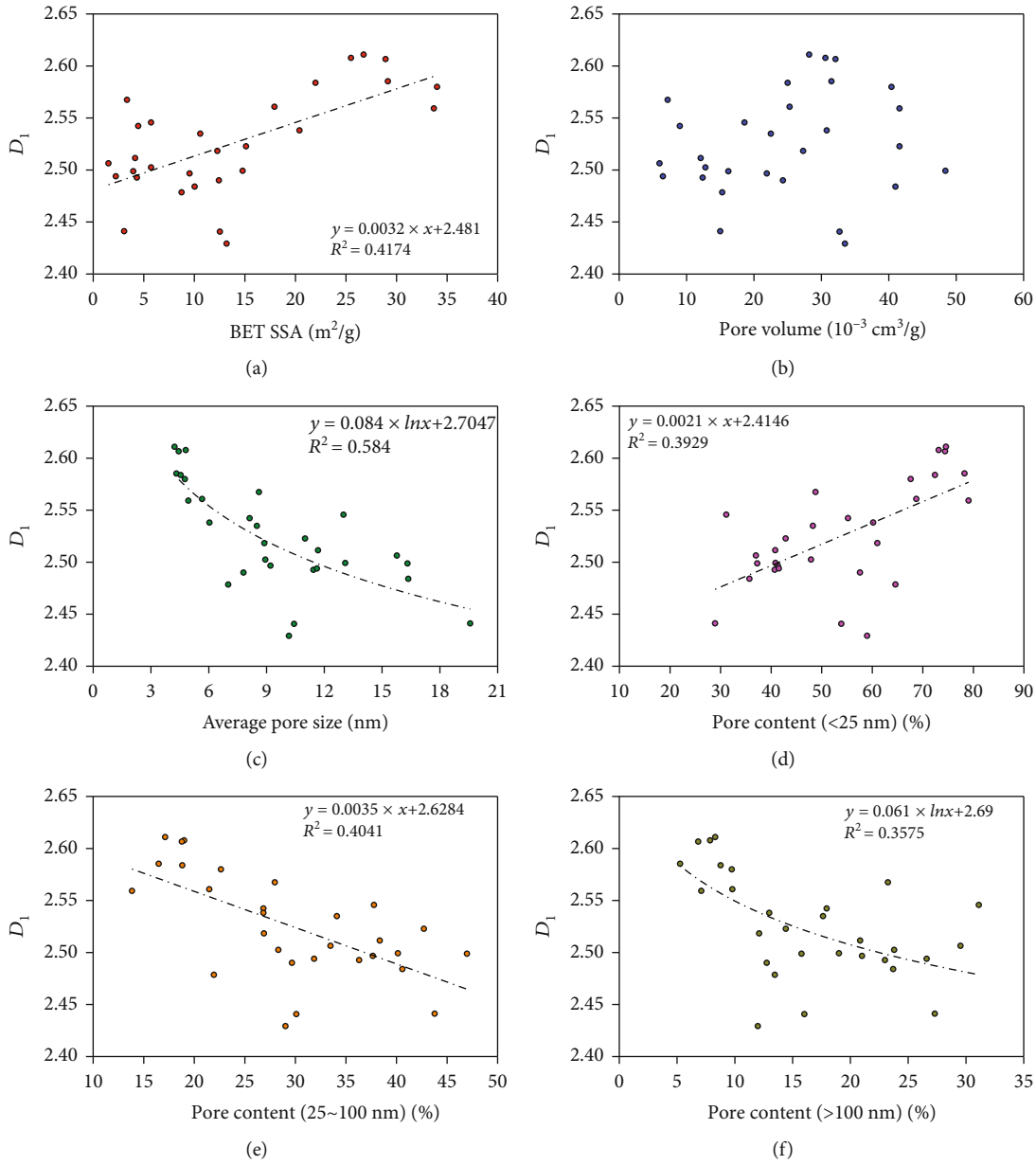

Figure 9: Relationships between D_1 and pore structure parameters.

In contrast, the slightly negative relationship between SSA and carbonate mineral content is illustrated in Figure 8(c). Carbonate minerals such as calcite and dolomite have a large number of dissolution pores, which are generally much larger than intragranular pores in clay minerals (Figure 4). Thus, the higher the carbonate mineral content is, the more dissolution pores there are, resulting in a lower SSA. The higher the content of pores larger than 25 nm, the lower the SSA is (as shown in Figure 7(a)). However, there is no apparent relationship between pore volume and carbonate minerals. The reason can be explained from Figure 7(b). Specifically, there is an obvious correlation between pores larger than 100 nm and pore volume but no apparent relationship between pore volume and pores of 25-100 nm, leading to pore volume not being correlated with carbonate minerals. Dissolution pores in calcite or dolomite are generally larger than 25 nm (Figure 4).

4.2. Factor Effects on Fractal Dimensions. The relationship between the pore structure parameters and the fractal dimensions is obvious in Figures 9 and 10. The fractal dimensions (D_1 and D_2) are positively correlated with the SSA but have no apparent relationship with pore volume. In contrast, there are negative relationships between the fractal dimensions and average pore diameter. The fractal dimensions decrease rapidly as the average pore diameter increases. This is because shales with smaller average pore diameters would also have

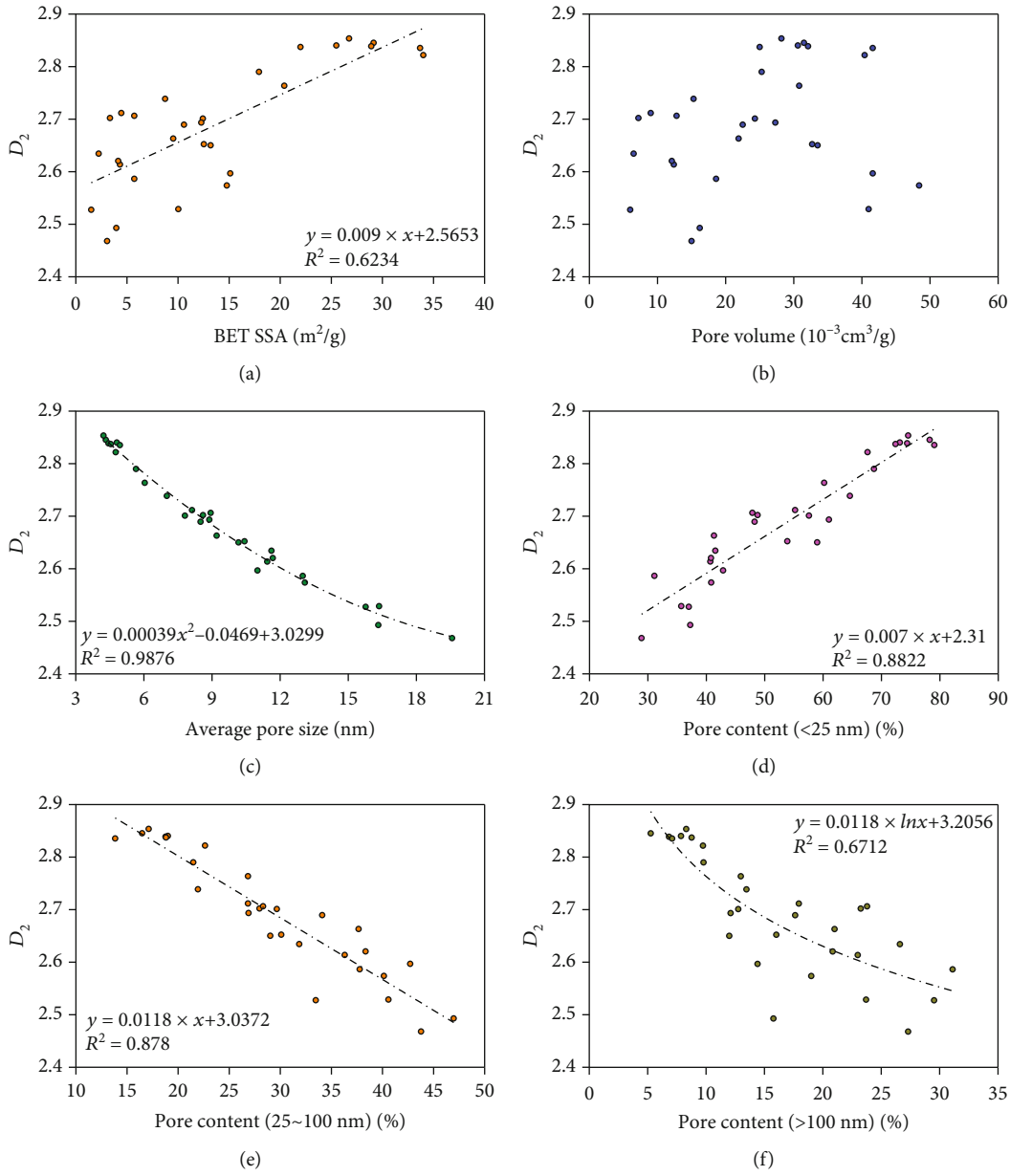

Figure 10: Relationships between D_2 and pore structure parameters.

more pores less than 25 nm but fewer pores large than 25 nm, resulting in that the SSA and fractal dimensions also increase.

To reveal the role of TOC and the mineralogical compositions of shale affecting the fractal dimensions, the correlations between fractal dimensions and TOC, clay minerals, and carbonate minerals are plotted in Figure 11. The relationship between the fractal dimensions (both D_1 and D_2) and TOC contents is characterized by a U-shaped curve, which is similar to the data of lacustrine shale from Qingshankou Formation documented by Wang et al. [12] but contrasts that of the aforementioned gas marine shale [13, 16]. For the gas marine shale, a parabola curve was observed between fractal dimensions and TOC content [16]. In this study, the U-shaped curve is characterized by a yielding point at 3.0% TOC content (3.0% is an approximation) when the fractal dimensions reach minimum values (Figures 11(a) and 11(d)). Specifically, when the TOC content is less than 3.0%, the fractal dimensions (D_1 and D_2) decrease as the TOC content increases. The reasons may be as follows. For shale in the oil window, there are few pores in the organic matter, resulting in the pore structure and surface being almost unaffected by organic matter. Thus, fractal dimensions would not increase as the TOC content increased. Moreover, the higher the organic matter content (TOC) is, the more organic acids are produced during the hydrocarbon generation process, leading to more large dissolution pores in the carbonated minerals [38], thus decreasing the fractal dimensions D_1 and D_2. Meanwhile, both D_1 and D_2 show

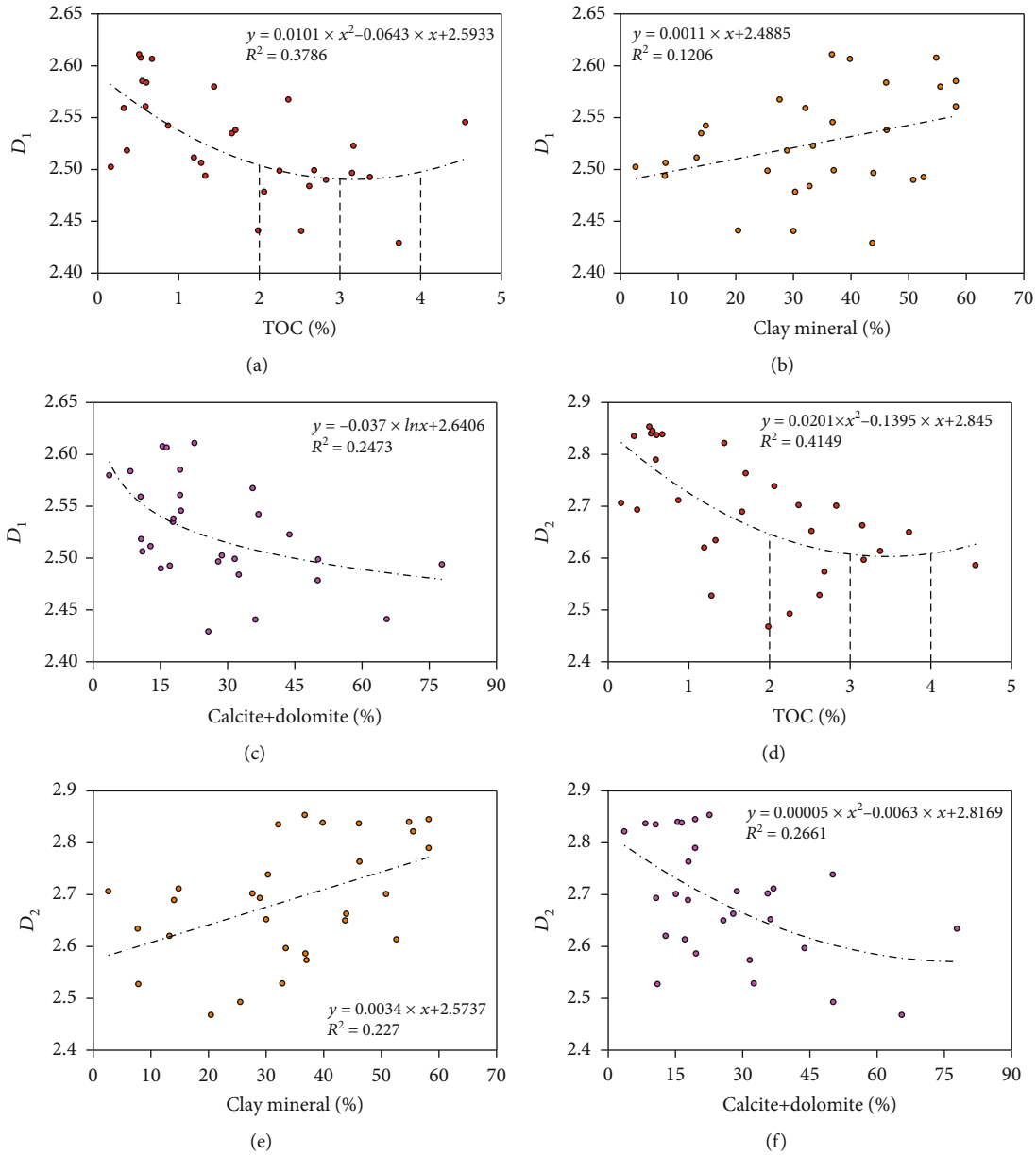

Figure 11: Relationships between fractal dimensions and TOC and mineralogical compositions.

negative relationships with carbonate minerals (as illustrated in Figures 11(c) and 11(f)). This is because shales with a higher carbonate mineral content generally produce larger pores due to dissolution.

When the TOC content is larger than 3%, the fractal dimensions eventually increase as the TOC content increases. The results may be that as a typical plastic substance, the higher the organic matter content is, the weaker the compressive resistance of shale, thus producing more complex smaller pores. Fractal dimensions (D_1 and D_2) were positively correlated with clay mineral content (Figures 11(b) and 11(e)). Clay minerals increase the SSA of shale due to their layer and flocculent structure (Figure 4), thus producing smaller pores and enhancing the complexity of the pore structure and surface. Hence, a higher clay mineral content leads to the higher fractal dimensions.

4.3. Oil Contents Controlled by Pore Structure and Fractal Dimensions. S_1 is the remaining hydrocarbon content in shale, which is generally used to characterize the shale oil content [3]. The OSI (oil saturation index, S_1/TOC × 100 mg/g) is widely used to characterize the mobility of shale oil [39]. In this paper, the relationships between these two parameters and pore structure and fractal dimensions were investigated (as shown in Figure 12). There are apparent negative relationships between SSA and S_1 and OSI, suggesting that shale samples with larger SSAs contain less free oil. The S_1 and OSI of the studied shales show an

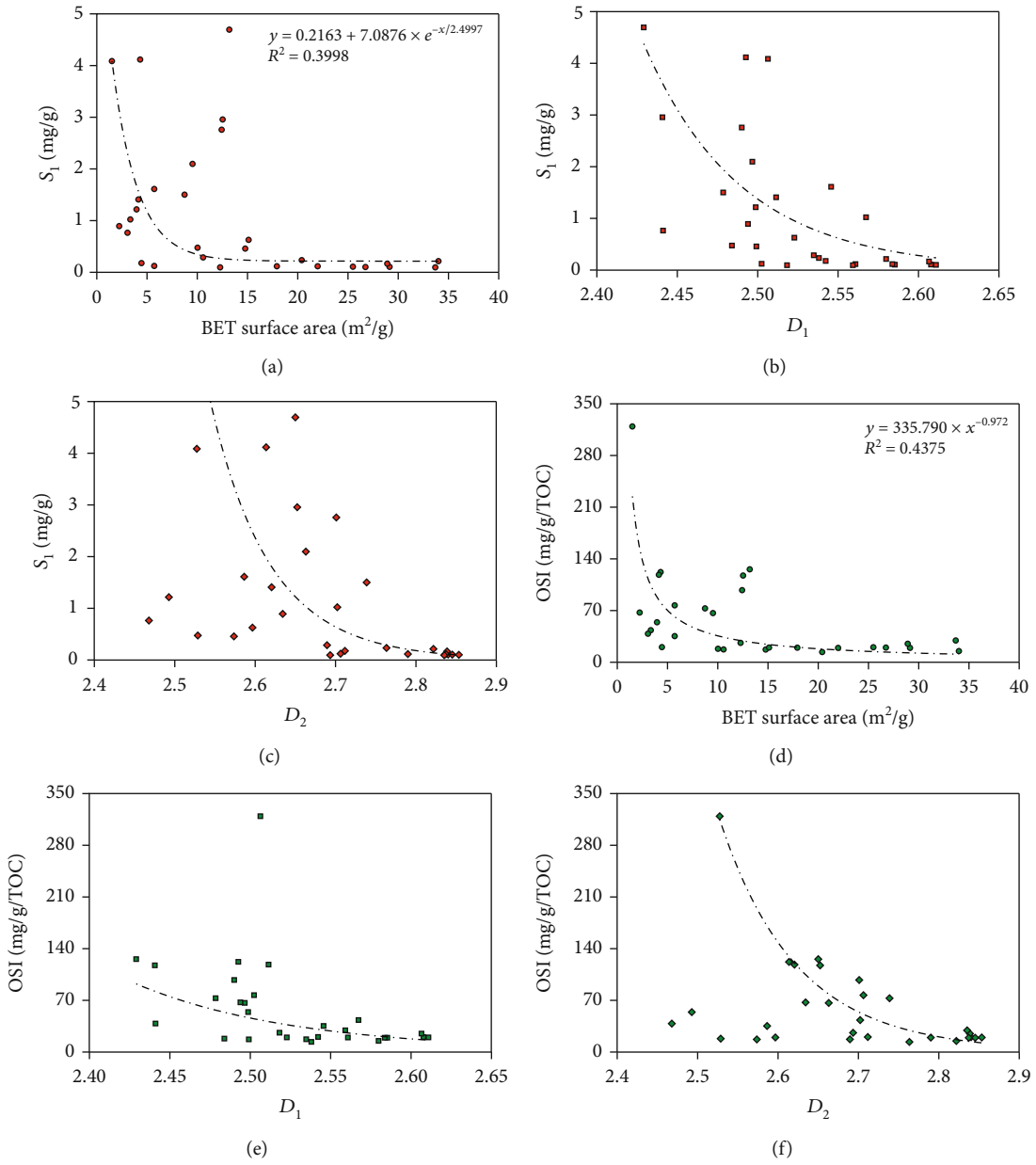

Figure 12: Relationships between oil content (S_1 and OSI) and pore structure and fractal dimensions.

apparently negative correlation with their fractal dimensions (both D_1 and D_2) (Figures 12(b), 12(c), 12(e), and 12(f)). Shale with higher levels of free oil generally has lower values of SSA and fractal dimensions. This phenomenon is inconsistent with gas shale. Gas shale with a larger SSA can provide more adsorption sites for gas molecules. Moreover, gas shale with higher fractal dimensions has a more irregular surface and complex pore structure, which are conducive to gas adsorption. Therefore, the gas adsorption capacity of gas shale increases as the SSA and fractal dimensions increase. Conversely, free oil mainly occurs in large pores; thus, lacustrine shale with a higher free oil content is commonly characterized by lower values of SSA and dimensions. Therefore, considering the influence of TOC on fractal dimensions and the correlations between fractal dimensions and S_1 and OSI, lacustrine shale in the oil window with a TOC content of 2%-4% is regarded as the optimal shale oil exploration target in the Shahejie Formation, Dongying Sag. This conclusion is consistent with that obtained from the Qingshankou Formation, Songliao Basin, so it can be concluded that lacustrine shale in the oil window with TOC contents of approximately 3% is probably the preferred shale oil exploration target.

5. Conclusions

In this paper, the following conclusions were reached.

(1) Lacustrine shales have different adsorption and fractal characteristics at relative pressures of 0-0.5 and 0.5-1. Two fractal dimensions (D_1 and D_2) were calculated by the FHH model based on the nitrogen adsorption branches. D_1 ranges from 2.4292 to 2.6109, with a mean value of 2.5245, while D_2 is between 2.4680 and 2.8535, with an average of 2.6889

(2) The average pore diameter has an apparent negative relationship with the specific surface area (SSA) but an apparent correlation with the pore volume. There is a positive correlation between pore volume and the SSA except for shales with many larger dissolution pores. The SSA and pore volume have no apparent relationship with the TOC content but a slightly positive correlation with the clay mineral content. Carbonate minerals show a slightly negative relationship with SSA but no apparent correlation with pore volume

(3) The fractal dimensions (both D_1 and D_2) of shales increase with increasing SSAs but with decreasing average pore diameters and have no correlation with pore volume. The relationships between fractal dimensions and TOC content are characterized by U-shaped curves, with a yielding point at 3% TOC content when the fractal dimensions are minimal. Moreover, both D_1 and D_2 were positively correlated with clay minerals but negatively correlated with carbonate minerals

(4) S_1 and OSI of shales rapidly decrease as the SSAs and fractal dimensions increase, so lacustrine shales with higher contents of free oil are generally characterized by lower SSA and fractal dimensions. The lacustrine shales in the oil window with TOC contents of 2%-4% are regarded as the preferred shale oil exploration target in the Shahejie Formation, Dongying Sag, and Bohai Bay Basin.

Data Availability

The data used to support the findings of this study are included within the article.

Conflicts of Interest

The authors declare that they have no conflicts of interest.

Acknowledgments

This work was financially supported by the Natural Science Foundation of Shandong Province (ZR2020QD036 and ZR2020QD037) and the National Natural Science Foundation (41972123, 41772131, and 41673066).

References

[1] C. N. Zou, D. Z. Dong, H. Yang et al., "Conditions of shale gas accumulation and exploration practice in China," *Nature Gas Industry*, vol. 31, pp. 26–39, 2011.

[2] B. Liu, J. H. Sun, Y. Q. Zhang et al., "Reservoir space and enrichment model of shale oil in the first member of Cretaceous Qingshankou Formation in the Changling sag, southern Songliao Basin, NE China," *Petroleum Exploration and Development*, vol. 48, pp. 1–16, 2021.

[3] S. F. Lu, H. T. Xue, M. Wang et al., "Several key issues and research trends in evaluation of shale oil," *Acta Petrolei Sinica*, vol. 37, pp. 1309–1322, 2016.

[4] W. B. Li, S. F. Lu, J. Q. Li et al., "Geochemical modeling of carbon isotope fractionation during methane transport in tight sedimentary rocks," *Chemical Geology*, vol. 566, p. 120033, 2021.

[5] J. C. Zhang, L. M. Lin, Y. X. Li et al., "Classification and evaluation of shale oil," *Earth Science Frontiers*, vol. 19, pp. 322–331, 2012.

[6] J. Q. Li, S. F. Lu, L. J. Xie et al., "Modeling of hydrocarbon adsorption on continental oil shale: a case study on n-alkane," *Fuel*, vol. 206, pp. 603–613, 2017.

[7] J. Q. Li, S. F. Lu, J. C. Cai, P. F. Zhang, H. T. Xue, and X. B. Zhao, "Adsorbed and free oil in lacustrine nanoporous shale: a theoretical model and a case study," *Energy & Fuels*, vol. 32, no. 12, pp. 12247–12258, 2018.

[8] R. G. Loucks, R. M. Reed, S. C. Ruppel, and U. Hammes, "Spectrum of pore types and networks in mudrocks and a descriptive classification for matrix-related mudrock pores," *AAPG Bulletin*, vol. 96, no. 6, pp. 1071–1098, 2012.

[9] B. Liu, Y. F. Gao, K. Q. Liu et al., "Pore structure and adsorption hysteresis of the middle Jurassic Xishanyao shale formation in the Southern Junggar Basin, northwest China," *Energy Exploration & Exploitation, vol*, vol. 39, no. 3, pp. 761–778, 2021.

[10] X. D. Yin, S. F. Lu, K. Y. Liu, S. Jiang, and B. Sun, "Non-uniform subsidence and its control on the temporal-spatial evolution of the black shale of the Early Silurian Longmaxi Formation in the western Yangtze Block, South China," *Marine and Petroleum Geology*, vol. 98, pp. 881–889, 2018.

[11] P. F. Zhang, S. F. Lu, J. Q. Li et al., "Broad ion beam-scanning electron microscopy pore microstructure and multifractal characterization of shale oil reservoir: a case sample from Dongying Sag, Bohai Bay Basin, China," *Energy Exploration & Exploitation*, vol. 38, no. 3, pp. 613–628, 2020.

[12] M. Wang, H. T. Xue, S. S. Tian, R. W. T. Wilkins, and Z. W. Wang, "Fractal characteristics of Upper Cretaceous lacustrine shale from the Songliao Basin, NE China," *Marine and Petroleum Geology*, vol. 67, pp. 144–153, 2015.

[13] F. Yang, Z. F. Ning, and H. Q. Liu, "Fractal characteristics of shales from a shale gas reservoir in the Sichuan Basin, China," *Fuel*, vol. 115, pp. 378–384, 2014.

[14] X. J. Liu, J. Xiong, and L. X. Liang, "Investigation of pore structure and fractal characteristics of organic-rich Yanchang formation shale in central China by nitrogen adsorption/-desorption analysis," *Journal of Natural Gas Science and Engineering*, vol. 22, pp. 62–72, 2015.

[15] J. G. Hu, S. H. Tang, and S. H. Zhang, "Investigation of pore structure and fractal characteristics of the Lower Silurian Longmaxi shales in western Hunan and Hubei provinces in China," *Journal of Natural Gas Science and Engineering*, vol. 28, pp. 522–535, 2016.

[16] A. Li, W. L. Ding, J. H. He, P. Dai, S. Yin, and F. Xie, "Investigation of pore structure and fractal characteristics of organic-rich shale reservoirs: a case study of Lower Cambrian

Qiongzhusi formation in Malong block of eastern Yunnan Province, South China," *Marine and Petroleum Geology*, vol. 70, pp. 46–57, 2016.

[17] A. Li, W. L. Ding, X. H. Zhou et al., "Investigation of the methane adsorption characteristics of marine shale: a case study of Lower Cambrian Qiongzhusi Shale in eastern Yunnan Province, South China," *Energy & Fuels*, vol. 31, no. 3, pp. 2625–2635, 2017.

[18] Y. Li, Z. S. Wang, Z. J. Pen, X. L. Niu, Y. Yu, and S. Z. Meng, "Pore structure and its fractal dimensions of transitional shale: a cross-section from east margin of the Ordos Basin, China," *Fuel*, vol. 241, pp. 417–431, 2019.

[19] J. He, S. He, Z. X. Liu et al., "Pore structure and adsorption capacity of shale in the Lower Cambrian Shuijingtuo Formation in the southern flank of Huangling anticline, western Hubei," *Acta Petrolei Sinica*, vol. 41, pp. 27–42, 2020.

[20] I. G. Torre, J. J. Martin-Sotoca, J. C. Losada, P. López, and A. M. Tarquis, "Scaling properties of binary and greyscale images in the context of X-ray soil tomography," *Geoderma*, vol. 365, p. 114205, 2020.

[21] Z. T. Li, D. M. Liu, Y. D. Cai, P. G. Ranjith, and Y. B. Yao, "Multi-scale quantitative characterization of 3-D pore-fracture networks in bituminous and anthracite coals using FIB-SEM tomography and X-ray μ-CT," *Fuel*, vol. 209, pp. 43–53, 2017.

[22] X. D. Yin, S. Jiang, Y. L. Li et al., "Impact of pore structure and clay content on the water-gas relative permeability curve within tight sandstones: a case study from the LS block, eastern Ordos Basin, China," *Journal of Natural Gas Science and Engineering*, vol. 81, p. 103418, 2020.

[23] X. D. Yin, S. Jiang, S. J. Chen et al., "Impact of rock type on the pore structures and physical properties within a tight sandstone reservoir in the Ordos Basin, NW China," *Petroleum Science*, vol. 17, no. 4, pp. 896–911, 2020.

[24] F. Zeng, C. M. Dong, C. Y. Lin et al., "Analyzing the effects of multi-scale pore systems on reservoir properties—a case study on Xihu Depression, East China Sea Shelf Basin, China," *Journal of Petroleum Science and Engineering*, vol. 203, p. 108609, 2021.

[25] P. F. Zhang, S. F. Lu, J. Q. Li, and X. C. Chang, "1D and 2D nuclear magnetic resonance (NMR) relaxation behaviors of protons in clay, kerogen and oil-bearing shale rocks," *Marine and Petroleum Geology*, vol. 114, p. 104210, 2020.

[26] H. L. Bu, Y. W. Ju, J. Q. Tan, G. C. Wang, and X. S. Li, "Fractal characteristics of pores in non-marine shales from the Huainan coalfield, eastern China," *Journal of Natural Gas Science and Engineering*, vol. 24, pp. 166–177, 2015.

[27] G. C. Wang and Y. W. Ju, "Organic shale micropore and mesopore structure characterization by ultra-low pressure N_2 physisorption: experimental procedure and interpretation model," *Journal of Natural Gas Science and Engineering*, vol. 27, pp. 452–465, 2015.

[28] N. D. Deng, B. R. Jiang, W. Gao, and W. Fu, "Study on pore structure and fractal characteristics of shale from coal measures of Longtan Formation in western Guizhou," *Coal Science and Technology*, vol. 48, pp. 184–190, 2020.

[29] L. Y. Zhang, S. Y. Bao, J. Y. Li, Z. Li, R. F. Zhu, and J. G. Zhang, "Movability of lacustrine shale oil: a case study of Dongying Sag, Jiyang Depression, Bohai Bay Basin," *Petroleum Exploration and Development*, vol. 41, pp. 701–711, 2014.

[30] Y. R. Zou, J. N. Sun, Z. Li, X. Y. Xu, M. W. Li, and P. A. Peng, "Evaluating shale oil in the Dongying Depression, Bohai Bay Basin, China, using the oversaturation zone method," *Journal of Petroleum Science & Engineering*, vol. 161, pp. 291–301, 2018.

[31] P. F. Zhang, S. F. Lu, and J. Q. Li, "Characterization of pore size distributions of shale oil reservoirs: a case study from Dongying sag, Bohai Bay basin, China," *Marine and Petroleum Geology*, vol. 100, pp. 297–308, 2019.

[32] B. B. Mandelbrot, *Les Objects Fractals: Forme, Hasard et Dimension*, Flammarion, Paris, 1975.

[33] Y. B. Yao, D. M. Liu, D. Z. Tang, S. H. Tang, and W. H. Huang, "Fractal characterization of adsorption-pores of coals from North China: an investigation on CH_4 adsorption capacity of coals," *International Journal of Coal Geology*, vol. 73, no. 1, pp. 27–42, 2008.

[34] Y. D. Cai, D. M. Liu, Z. J. Pan, Y. B. Yao, J. Q. Li, and Y. K. Qiu, "Pore structure and its impact on CH4 adsorption capacity and flow capability of bituminous and subbituminous coals from Northeast China," *Fuel*, vol. 103, pp. 258–268, 2013.

[35] S. F. Lu, W. B. Huang, F. W. Chen et al., "Classification and evaluation of shale oil and gas resources: discussion and application," *Petroleum Exploration and Development*, vol. 39, pp. 249–256, 2012.

[36] S. J. Gregg and K. S. W. Sing, *Adsorption, Surface Area and Porosity*, Academic Press, New York, Second edition, 1982.

[37] P. F. Zhang, S. F. Lu, J. Q. Li, H. T. Xue, W. H. Li, and P. Zhang, "Characterization of shale pore system: a case study of Paleogene Xin'gouzui Formation in the Jianghan basin, China," *Marine and Petroleum Geology*, vol. 79, pp. 321–334, 2017.

[38] D. M. Jarvie, "Shale resource systems for oil and gas: part 2 –shale-oil resource systems," *AAPG Memoir*, vol. 97, pp. 89–119, 2012.

[39] S. Li, S. Hu, X. Xie, Q. Lv, X. Huang, and J. Ye, "Assessment of shale oil potential using a new free hydrocarbon index," *International Journal of Coal Geology*, vol. 156, pp. 74–85, 2016.